PNAS

RESEARCH ARTICLE | APPLIED PHYSICAL SCIENCES

Learning nature's assembly language with polymers

Oliver Xie[a], Alexander E. Cohen[a], Martin Z. Bazant[a], and Bradley D. Olsen[a,1]

Edited by Frank Bates, University of Minnesota Twin Cities, Minneapolis, MN; received July 18, 2025; accepted December 5, 2025

The self-assembly of matter into ordered structures is ubiquitous throughout nature and engineered systems. Programming a material's macroscopic properties via molecular-level structural control is a grand scientific challenge, requiring methods for inverse design that can design a targeted molecule to achieve a given self-assembled structure. One model system that serves as a common proving ground for inverse design algorithms is block copolymers. In these systems, self-consistent field-theory (SCFT) provides a robust thermodynamic model for predicting self-assembly for a given molecular sequence. This work presents a computational algorithm which learns the reverse translation, allowing a target structure to be achieved by varying molecular sequence. The algorithm is based on development of an adjoint solution of the SCFT equations allowing incorporation of automatic differentiation. The power of this algorithm is demonstrated by inverse designing polymer sequences to yield equilibrium structures, resolving the long-standing dilemma of navigating the combinatorial explosion of sequence possibilities offered by complex copolymer designs. The inverse designed sequences show that the algorithm learns to modulate unfavorable block interactions to stabilize these complex morphologies. By learning how to program self-assembly at the molecular-level using only a thermodynamic model, this work opens the door to similar computational inverse design across other soft matter systems.

block copolymer | self-assembly | inverse design

Significance

Self-assembled structures in soft matter systems yield macroscopic material properties and result from an intricate thermodynamic balance. In block copolymers, molecular-level sequence changes result in different equilibrium microstructures. The large sequence design space makes finding new microstructures a grand challenge. Computational inverse design can be used to resolve this challenge. Here, an algorithm was developed which learns how sequence changes affect microstructure via automatic differentiation of the self-consistent field-theory (SCFT) thermodynamic model. This algorithm was validated by inverse designing the O^{70} network phase in a diblock copolymer. Two central questions in copolymer physics were addressed with this algorithm: 1) can sequence-control be leveraged to stabilize complex microstructures, and 2) is there a minimum block number necessary for forming a microstructure.

Molecules such as proteins, lipids, polymers, amphiphiles, and liquid crystals can self-assemble into ordered structures where the equilibrium structure is determined from solely molecular properties via the laws of thermodynamics. Molecular configuration in structured assemblies gives rise to emergent properties which nature takes advantage of in a myriad of ways. Toughness from complex ordering of cellulose gives trees its strength (1–3), the assembly of photonic crystals into a single gyroid colors butterfly wings and bird feathers (4–7), and the organization of membraneless biomolecular condensates from DNA–protein interactions drives transcription processes central to life (8–12).

Inspired by nature, programming soft matter material properties through the design of ordered structures with molecular-level chemical control has been explored for a variety of applications (13–19). This task is commonly known as inverse design and is recognized as one of the grand interdisciplinary challenges in soft materials, polymers, and supramolecular chemistry (20–22). In polymer systems, inverse design has been successfully applied to design polymers with desired thermal conductivities (23), mechanical toughness (23, 24), rheological properties (25), and glass transition temperatures (26). Several of these properties are the result of self-assembled structures. A model polymer system for studying self-assembly is a block copolymer melt (27, 28). Decades of experimentation have shown their self-assembly into a variety of complex mesoscale ordered microstructures (29–31). The interplay of monomer immiscibility due to chemical dissimilarity constrained by chain connectivity on a single copolymer leads to self-assembled microdomains rich in a particular monomer species. This thermodynamic balance is tunable by monomer-level control over the copolymer sequence's chemistry, leading to different equilibrium structures (32).

In copolymer systems, inverse design optimizes the inputs to the system, for example the polymer chain sequence, molar mass, or surface boundary conditions, in order to achieve a targeted microstructure or property result. Computational inverse design of copolymers to achieve novel microstructures has been extensively investigated. The importance of incorporating physics-based models in inverse design has been highlighted in other disciplines (33–35), and several works use particle-based molecular dynamics as the model (23, 36, 37). Another common physics-based model is field-theoretic simulations, specifically self-consistent field theory (SCFT), to perform the sequence-to-structure predictive task. SCFT stems from the seminal works of Helfand (38, 39) and later advancements by Matsen, Schick, Fredrickson, Morse, and numerous other researchers have turned it into a widely adopted computational tool which has successfully been used to interpret experimental scattering results, delineate phase boundaries, and validate structures as equilibrium or

Author affiliations: [a]Department of Chemical Engineering, Massachusetts Institute of Technology, Cambridge, MA 02139

Author contributions: O.X. and B.D.O. designed research; O.X. and A.E.C. performed research; A.E.C. and M.Z.B. contributed new computational tools; O.X. analyzed data; and O.X. and B.D.O. wrote the paper.

The authors declare no competing interest.

This article is a PNAS Direct Submission.

[1]To whom correspondence may be addressed. Email: bdolsen@mit.edu.

This article contains supporting information online at https://www.pnas.org/lookup/suppl/doi:10.1073/pnas.2519094123/-/DCSupplemental.

metastable (40–51). Incorporation of SCFT into an inverse design workflow has been investigated by numerous researchers. One successful workflow is to converge the equilibrium microstructure of a guessed sequence using SCFT, modify the sequence with an algorithm using the results of SCFT, then converge the new sequence with SCFT (52–57). This is conducted iteratively until the target microstructure is found.

A critical step in this scheme is determining how the results of SCFT simulations inform the next sequence change. Various algorithmic approaches, including particle swarm optimization (52, 53), evolutionary algorithms (56–58), and Bayesian optimization of a surrogate function (55) have been explored for this step. A limitation of these algorithms is that the gradient information of how the SCFT-converged solution is affected by sequence changes is not used in the design process. Without this, interpolation within sampled points on the design space is required to find the desired microstructure. For low-dimensional design spaces such as those formed by linear diblocks or triblocks, this is a minor limitation; however, for higher-order multiblock copolymers, the design space which must be sampled grows prohibitively large for these methods.

Direct incorporation of the gradient information from SCFT has proven challenging, since the solution of the SCFT equations requires an iterative relaxation of high-dimensional field variables such that nonlinear equations and partial differential equations are satisfied. Recent inverse design works have attempted to replace these equations with an easier-to-differentiate neural network (59, 60). The use of neural networks requires high confidence that the neural network faithfully reproduces the SCFT results for any possible sequence design. Given the large sequence design landscape, much of which remains unexplored, this cannot be guaranteed.

This work presents an algorithmic solution to inverse design which directly incorporates gradient information of the SCFT equations in informing sequence changes. In this manner, the algorithm "learns" the structure-to-sequence translation within the SCFT thermodynamic model without the need for surrogate functions. To do so, it uses the adjoint solution of SCFT with reverse-mode automatic differentiation (AD) to design a sequence which yields a target microstructure while satisfying the thermodynamic model. A second part of the algorithm then performs negative selection of the microstructure against other candidate structures, adjusting the sequence to bring the target into equilibrium (Fig. 1).

The power of directly incorporating the thermodynamic model into inverse design was demonstrated by addressing two complex questions in block copolymer self-assembly. First, can precise sequence control decrease the number of blocks required to access a complex phase? Second, is there a minimum number of blocks required for a block copolymer to obtain a new complex microstructure? The computational and experimental costs of a brute force search through the design space of possible copolymer sequences have prevented prior attempts to answer these questions (61). This obstacle is surmounted with direct incorporation of the SCFT thermodynamic model into inverse design, allowing the algorithm to learn the microstructure-to-sequence relation and unlocking for the first-time physics-guided navigation of the design space.

Methods

Self-Consistent Field Theory. A previously published SCFT formalism incorporating a sequence function description was used here (62). The sequence-SCFT model uses a vector-valued sequence function $\boldsymbol{f}(s)$ defined along the contour s of the copolymer. Each dimension n of $\boldsymbol{f}(s)$ can correspond to a different chemical property, such as Hildebrand or Hansen solubility parameters (63). This allows a flexible and differentiable sequence representation for the multiblock and tapered multiblock copolymers used in this work, as described in *SI Appendix*. An interaction model generates a symmetric matrix Λ of intermonomer interaction parameters; for multiblock copolymers, this is analogous to the χN parameter. In this work, the interaction model is the mean squared difference (Eq. **1**), and for all designs $n = 3$ was used, inspired by the three-dimensional Hansen parameters. Three adjustable fields are present in SCFT–the normalized density field ψ, the chemical potential field ω, and the Lagrangian multiplier field Ξ for enforcing incompressibility. In sequence-SCFT, the ψ and ω fields are defined for all spatial points in the simulation box and every contour point of sequence. The Ξ field is only spatially defined. The unit cell is also equilibrated during simulation with the method of Tyler and Morse (43).

$$\Lambda(s_1, s_2) = \frac{1}{n}\sum_{i}^{n}\left(f_i(s_1) - f_i(s_2)\right)^2. \qquad [\mathbf{1}]$$

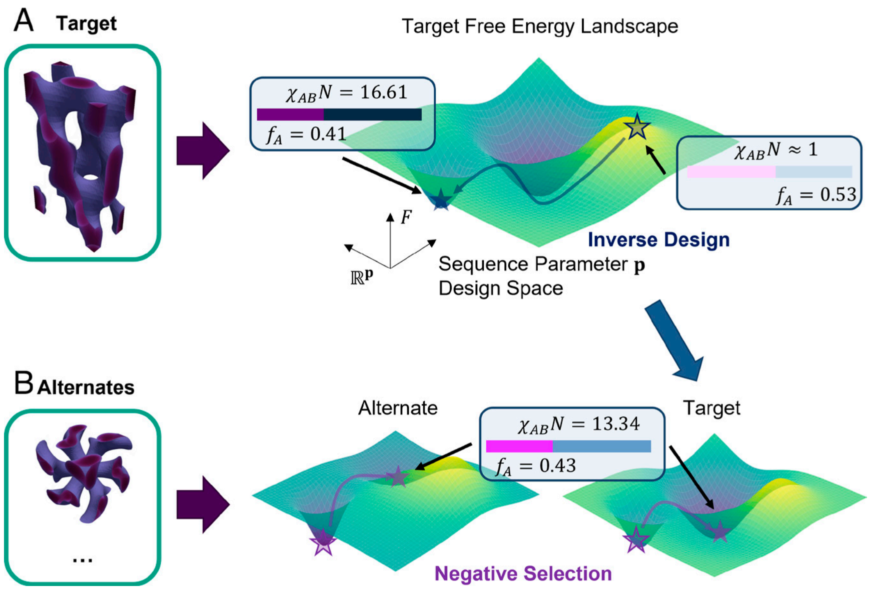

Fig. 1. Inverse design learns how self-assembly is coded into molecular-level properties. (*A*) For copolymer melts, inverse design optimizes design levers associated with chemical details of the monomers as well as sequence patterning in order to bring the desired microstructure into equilibrium on the free energy landscape. (*B*) Often times, this requires not just stabilizing the desired structure but also shifting the equilibrium phase (i.e., lowest energy phase) from another solution to the desired target using negative selection.

Here, space group symmetries are enforced not solely in reciprocal space but also in real space in order to reduce the number of points that must be solved. The smallest subset of coordinates (real space) or waves (reciprocal space) that can generate a unit cell given the symmetries are the asymmetric unit and irreducible Brillouin zone (BZ) respectively. By only storing the field values for these points, the dimensionality of the SCFT field variables to store and solve can be reduced. Inspired by the work of Qiang and Li, the SCFT fields are directly converted from the asymmetric unit to the irreducible BZ, bypassing the full spatial and wave representations (64). This conversion occurs via matrix multiplication using a precomputed coefficient matrix.

Computational Details. All calculations were done in Python using the JAX library. Calculations were performed in float64. Initial guess generation is important for SCFT, and here initialization relies on seeding structural features corresponding to the lowest noncancelled Fourier modes. Full details of this implementation are given in *SI Appendix*. The simulation cell was meshed as 32 × 32 × 32 (cubic and orthorhombic space groups), 36 × 36 × 24 (tetragonal space groups), 24 × 24 × 36 (hexagonal space groups), 48 × 48 × 1 (2D space groups), and 48 × 1 × 1 (1D space groups). This resolution is lower than many similar SCFT works; however, simulation of the gyroid structure showed little difference in free energy between a higher 48 × 48 × 48 discretization (*SI Appendix*). While a higher discretization is possible, there is a much higher memory requirement, especially in the GPU-accelerated AD steps used in the algorithms here. A gradient checkpointing method has been implemented to alleviate the memory requirements. The details of this algorithm are described in *SI Appendix*.

Initial cell lengths were set to 1 for 1D space groups, 2 for 2D space groups, and 3 for 3D space groups. This length was scaled accordingly if the spatial grid contains more points in one direction than the others, as is the case for the tetragonal and hexagonal systems. Calculations were performed on a single NVIDIA H200 GPU located in the Engaging Cluster at MIT. The Adam or AMSGrad optimizer were used for autograd optimization. The learning rates and hyperparameters used are detailed in *SI Appendix*.

Results and Discussions

Inverse Design with Direct Incorporation of SCFT. To develop an adjoint solution to the inverse design problem, the SCFT algorithm must be reformulated as a loss-minimization problem, achieving simultaneous solution of the self-consistent equations and inverse design toward a target simply via modification to the form of the loss function. This overcomes a limitation of prior SCFT algorithms which rely on gradient-free mixing schemes such as Anderson acceleration in inverse design. Gradient-free solutions to SCFT make it difficult to incorporate gradients of the microstructure with respect to sequence changes; this is a necessary prerequisite to using SCFT directly in calculating the loss function. Here, the iterated variables were the density field $\psi(\mathbf{x}, s)$, the Lagrangian multiplier field $\Xi(\mathbf{x})$, and the unit cell parameters θ. To solve the coupled modified diffusion equations (MDEs) in SCFT, the pseudospectral method was used (47). The symmetries of the space group are used to generate reduced representations of the field variables. The loss function was then constructed using the mean square error (MSE) of the evaluated fields from the self-consistency condition. Minimizing this MSE is analogous to finding a self-consistent solution. It was observed that with this scheme, there is a tendency for structures in low-symmetry space groups to collapse into structures with higher symmetries given a poor initial guess. For this reason, initializations of complex low-symmetry structures (such as Frank-Kasper structures) are taken from open-source SCFT solvers (45). To extend this methodology to inverse design, the parameters describing the copolymer sequence form another set of iterated variables, while the loss function now includes the MSE of the difference between the calculated density field and target microstructure density field. A few variations of this scheme were used for improved convergence to equilibrium morphologies, as detailed in *SI Appendix*.

Minimization of the loss function proceeds with automatic differentiation (AD) of the loss function with respect to the iterated parameters. Due to the MDEs at the core of SCFT, the minimization of loss with AD is equivalent to the adjoint solution method. The use of the adjoint solution of a physics-based model for inverse designing properties has recently been demonstrated in photonic device design and has proven more effective than methods which do not directly learn inversion through the physics model (65). These alternate methods include genetic algorithms, swarm optimization, or surrogate function methods such as Bayesian optimization, all of which form the prior state-of-the-art in copolymer microstructure inverse design (52, 55–58, 66). With modern optimizers and GPU acceleration, the adjoint implementation of SCFT described here is fast and converges to the same solutions as those calculated by classical SCFT algorithms (*SI Appendix*). The results show that the magnitude of difference between the normalized free energy of the adjoint-SCFT solution and highly converged Anderson-mixing SCFT solution is on the order of 10^{-4} when the loss function reaches around 10^{-7}. All calculated structures in this work are refined to at least this level of accuracy.

The inverse design of a sequence which forms the target microstructure as a self-consistent solution is necessary but insufficient for programming self-assembly into the copolymer sequence. Experimentally accessing a predicted microstructure requires that the structure is the equilibrium or at minimum a close metastable candidate. Therefore, the free energy of the target microstructure should be below that of all other candidate structures. This was achieved by the second part of the algorithm which performs negative selection against undesired alternate microstructures. The developed negative selection algorithm is analogous to bilevel optimization found for hyperparameter optimization in ML workflows (67). Bilevel optimization consists of two nested optimization loops. Here, the inner optimization enforced the self-consistency requirements for both the target microstructure and alternate candidate structures by running adjoint-SCFT. Alternate candidate structures were only considered in high symmetry space groups to prevent the previously described tendency for the solver to collapse structures to high symmetries. The free energies of the self-consistent structures were calculated. The loss function of the outer optimization generates a penalty if the free energy of the desired microstructure is higher than that of the alternate candidate structures. Gradient-based optimizers were used with AD to minimize this loss function by adjusting the sequence parameters, allowing selection both for a desired target and against undesired alternatives. Full details of this implementation are provided in *SI Appendix*.

Inverse Design of Diblock Sequence for Generating an Equilibrium O^{70} Network. A demonstration of the inverse design with negative selection algorithm is shown in Fig. 2, where a diblock sequence was successfully designed to yield the O^{70} network morphology as its equilibrium structure. The O^{70} network represents a difficult target with a narrow stability window spanning just 0.06 in block fraction and a χN range of about 4 (68). All other diblock microstructures serve as competing structures, and the sequence is close to the SCFT-predicted order–disorder transition.

Inverse design starts with a randomly generated copolymer, here corresponding to a very low $\chi_{AB}N$ and near symmetric diblock deep in the disordered region (Fig. 2*E*). The inverse design targets an O^{70} structure generated from a $\chi_{AB}N = 17.5$, $f_A = 0.38$ diblock motif; this structure is stable but not an equilibrium structure for the given block design. Correspondingly, inverse design successfully learned the sequence parameters which yield this morphology as a stable but not equilibrium microstructure (Fig. 2 *A* and *E*). In addition, inverse design was able to learn the cell lengths of the

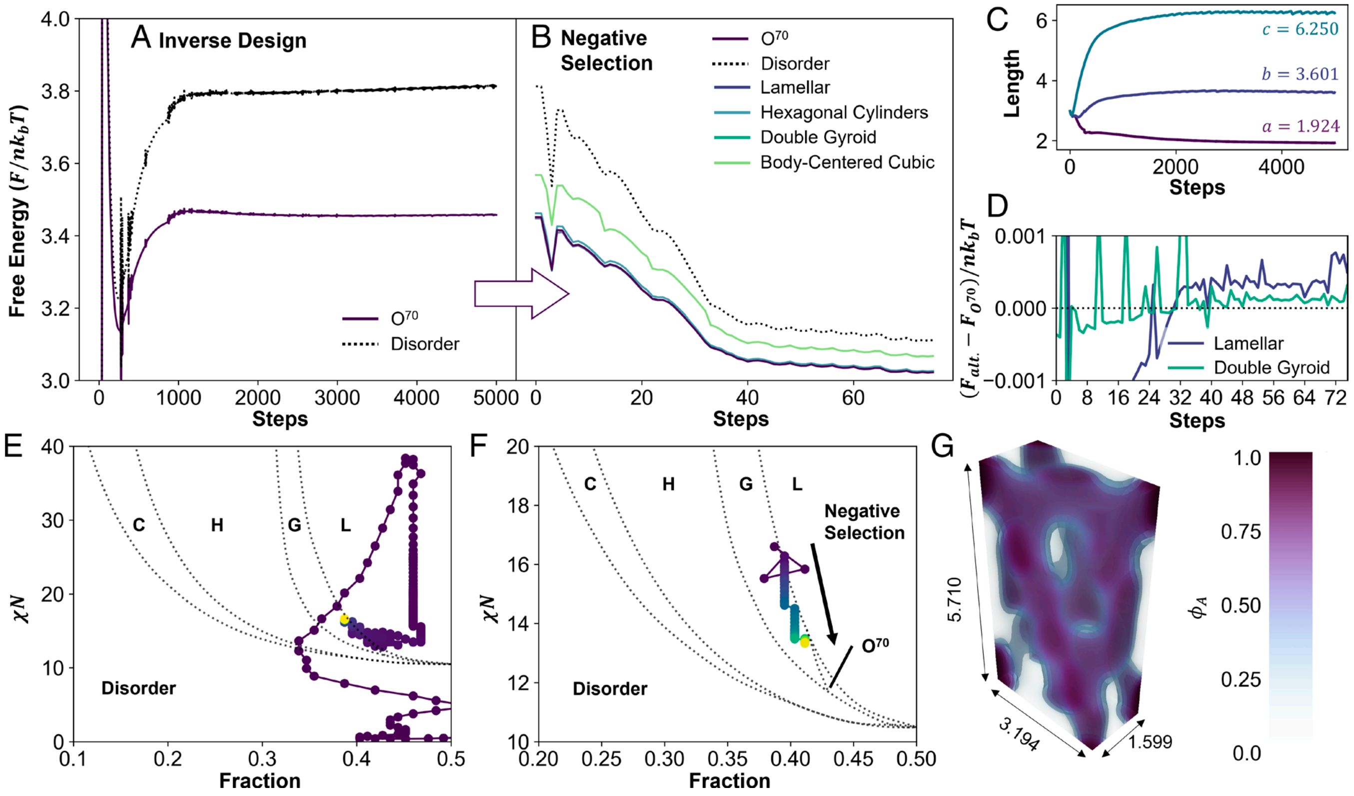

Fig. 2. A full run of inverse design and negative selection is shown to generate a stable O^{70} phase in a diblock-like copolymer. (*A*) The inverse design (without consideration of alternate formable structures) started from a randomly generated copolymer sequence and aims to converge the target O^{70} solution as a stable solution. The evolution of the free energy shows the formation of a highly stable structure. (*B*) Negative selection was performed to bring the O^{70} phase into equilibrium. (*C*) The cell length parameters are initially set to be 3 but over the course of inverse design naturally converge to a ratio close to that found for the O^{70} phase, without ever specifying a target value. (*D*) A close up of the free energy of alternate structures subtracted by the free energy of the O^{70} shows that at the final step, all alternate structures have a lower free energy. (*E*) The trajectory of the design parameters during inverse design mapped to a diblock phase diagram is shown (68, 69). The color corresponds to iteration number and approaches yellow as the iteration reaches the final step. Because the supplied O^{70} target was formed from a $f_A = 0.38$, $\chi N = 17.5$ diblock and is not an equilibrium structure, inverse design converges the sequence to exactly this point. (*F*) Negative selection brings the sequence toward an equilibrium region for O^{70}. The slight interblock tapering induced by the sigmoids used by the sequence function to approximate blocks was the origin of the slight (~0.01) difference in block fraction between the diblock region of O^{70} stability reported by Tyler and Morse (68) and the sequence found here. (*G*) The structure of the stable O^{70} structure of the negatively selected sequence is shown after additional SCFT refinement to ensure the self-consistent equations are satisfied.

unit cell. Starting from an initial 1: 1: 1 ratio, the algorithm converges to a unit cell ratio closer to that which stabilizes the O^{70} phase (Fig. 2).

From the inverse designed sequence, alternate structures in the space groups yielding the four common diblock phases ($P-1$, $p6mm$, $Ia-3d$, $Im-3m$) were generated and passed into the negative selection algorithm. For this example, negative selection does not enforce convergence to the supplied target morphology since the original target was metastable. Instead, the loss function penalizes the free energy of the microstructure in the target space group (*Fddd*) being higher than that of the alternate structures. After 76 steps of negative selection, the free energy of the O^{70} structure is below that of the two close competing phases of lamellar and double gyroid by 0.01% (prescribed as the tolerance), and the algorithm was stopped (Fig. 2*B*). Additional refinement of the converged solutions confirms that the O^{70} is the equilibrium structure. Fig. 2 *E* and *F* show the trajectories taken by the algorithm through the diblock design space for inverse design and negative selection respectively. The final designed sequence resides at one corner of the O^{70} window; the slight discrepancy between the overlaid diblock phase diagram and the converged sequence is due to the representation of block copolymers used in this work. To ensure differentiability of design variables, the sigmoid approximation of the block copolymer interfaces introduces a slight tapering into the sequence which means all multiblock copolymers studied here do not have perfectly sharp block interfaces. Nevertheless, the final converged sequence is extremely close to the double gyroid–lamellar–O^{70} triple point and represents a successful run of the inverse design with negative selection algorithm (68). The resulting structure (Fig. 2*G*) is characteristic of the O^{70} network phase and has ratios of unit cell lengths in close agreement to the reported $1{:}\,2{:}\,2\sqrt{3}$ (68).

Sequence-Level Control Encodes Near-Equilibrium Frank-Kasper Microstructures. Recently, advances in polymer synthesis have enabled increasing control over the copolymer sequence. However, a key question remains in whether this increased sequence control yields a corresponding increase in the number of complex microstructures that can be stabilized (32, 70–72). At one extreme, nature's biopolymers possess high sequence control which determines their self-assembly into ordered domains. Mimicking this control in engineered copolymers has been cited as a possible path toward more complex microstructures (70, 71). The foundational question addressed here is that of a minimal sequence complexity necessary to achieve a complex microstructure. However, unlike multiblock copolymers where the number of blocks is a good indicator for sequence complexity, full sequence-control presents a high-dimensional design space with a near infinite degree of complexity possible.

Here, a simple example of sequence control to create complex copolymers is presented via the use of linear statistically tapered copolymers which form blocks of chemically "blended" regions. This is a simple first extension beyond block copolymers, where the notion of "blocks" is preserved but where each block contains a taper. The strength of this taper for each block forms another set of parameters to be inverse designed. Tapered copolymers have been experimentally shown to expand the double gyroid microstructure stability window in diblocks, a result confirmed by SCFT (73, 74). Yet no new space groups have been stabilized through tapering. The challenge again lies in navigating the design space, even for this modest level of sequence-control, the sequence possibilities are even greater than that of block copolymers.

The inverse design algorithm was used again to address this question. The target structures are four complex Frank-Kasper spherical phases, three of which have previously been observed in block copolymer systems (A15, C15, C14) and an additional phase not yet reported in soft matter systems (C36) (50, 75, 76). It is noted that the Frank-Kasper σ phase was not simulated or designed for. The large grid size (often 128 × 128 × 72) required for accurately modeling the many interfaces of the σ phase exceeded available memory. Improvements in GPU computation, including parallelized GPU calculations, and new advances in large-scale fast Fourier transform (FFT) algorithms are promising in overcoming this barrier (77–79), and higher-performance computing resources could also enable larger grid sizes to be used. Not having a sufficiently refined grid size can result in the algorithm not converging to the desired structure, or returning inaccurate free energy calculations.

For diblocks, conformational asymmetry between the blocks is a requirement for accessing the Frank-Kasper phases in order to compensate for the unfavorable packing and stretching of the spherical domains (76, 80, 81). The corona is composed of the majority block, which is conformationally stiffer and stabilizes the unfavorable sphere packing over the more favorable packings of the classical structures (82). However, it is well known that tapers can stabilize thermodynamically unstable network phases by alleviating chain packing frustration by broadening the interface (81).

Diblock and triblock tapered block copolymers were inverse designed and negatively selected toward the four Frank-Kasper structures. While no sequence achieved an equilibrium Frank-Kasper microstructure with linear tapering, the tapered block copolymers did achieve close metastable configurations (Fig. 3*B*). Some of the closest metastable structures, such as the A15 Laves phase with the tapered diblock, were within 10^{-3} to 10^{-4} in normalized free energy to the closest competing microstructure. While not thermodynamically equilibrium, metastable structures which are very close in free energy to the equilibrium structure still represent viable targets through kinetically controlled processing (83–85).

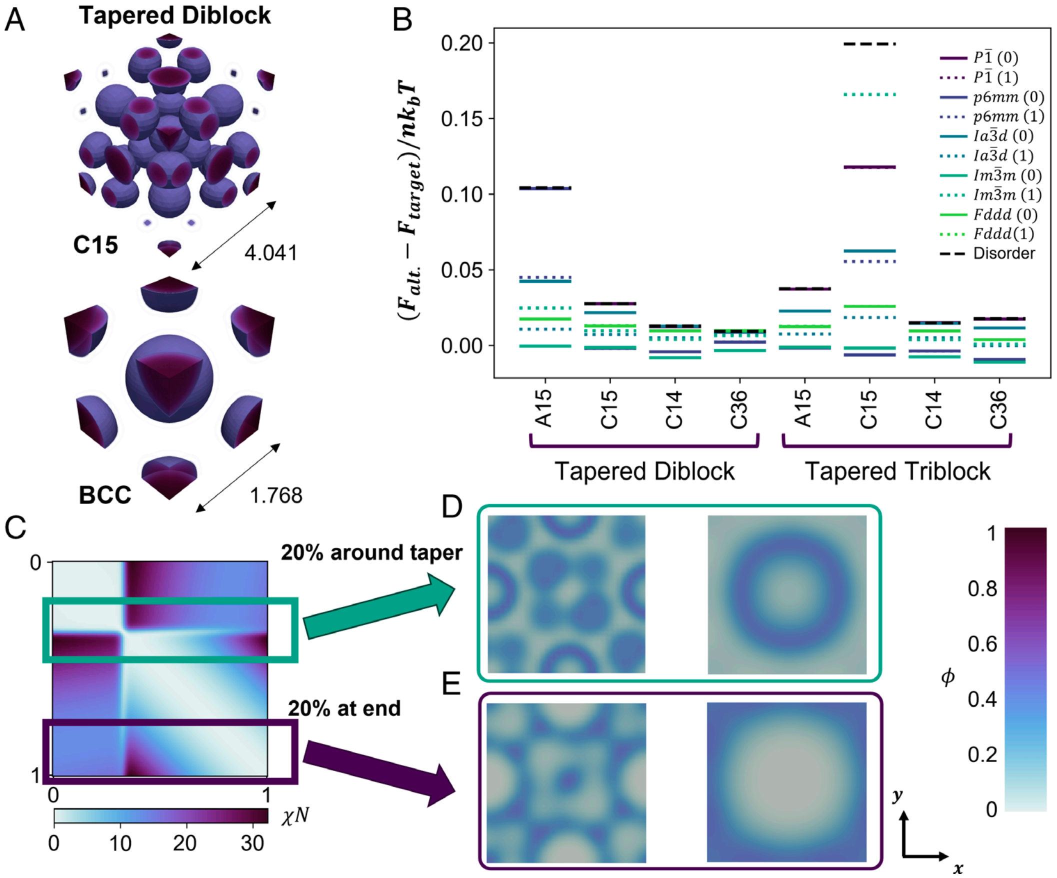

Fig. 3. Tapering was used to stabilize several Frank-Kasper microstructures. While none of the targets were found to be equilibrium, the use of tapering did bring several of the microstructures into a close metastable state. (*A*) For example, one such structure formed by a tapered diblock is the C15 Laves structure which is metastable, while a more stable alternate structure for the same sequence is the BCC spherical structure. The unit cell lengths of the resulting converged sequences are shown. (*B*) The difference in free energy between the Frank-Kasper target structures and alternate candidate structures are shown for inverse designed and negatively selected tapered diblock and tapered triblock sequences. 50 iterations of negative selection were used. For the diblock, without tapering inverse design was not successful for any of the Frank-Kasper structures, highlighting the ability of sequence complexity to access complex structures. (*C*) The sequence which forms the C15 Laves structure shown in (*A*) results in the interaction matrix as shown. The tapering introduces a strongly unfavorable interaction at the block interface, but also between the interface and the end of the second block. (*D* and *E*) The spatial distribution is shown for a 20% fraction of the total copolymer centered around the interface and the end. The sliced profiles are views of the x-y plane at 0.5 of the total z-plane height.

The mechanism for stabilizing the Frank-Kasper phases via tapering is examined with the C15 Laves phase (Fig. 3*A*). The interaction matrix of the designed sequence indicates a strong interaction penalty not only across the block interface, but also between the interface and the end of the second block (Fig. 3*C*). These two interaction penalties are hypothesized to act in a similar manner as conformational asymmetry in enabling corona stiffness. The full ψ field is integrated for 20% of the total copolymer length, once centered around the interface and once at the end of the second block. The resulting ϕ density field is plotted to analyze its spatial distribution. A slice of the C15 Laves microstructure as well as the more stable BCC spherical structure in the x-y plane taken at the midpoint of the unit cell is shown for each of the two ϕ fields (Fig. 3 *D* and *E*). The interparticle corona is composed of the interface and endblock, with each strongly localized in space forming shells around the particle. This localization requires entropically unfavorable chain stretching. In this system, tapering acts oppositely than the mechanism hypothesized in gyroid stabilization (73, 74); instead of broadening the interface, it is spatially localized with the entropic penalty offset by the unfavorable interaction of the block interface region with both ends of the polymer.

The inverse design algorithm could not resolve any untapered diblock sequence which yielded a self-consistent and stable target Frank-Kasper structure. This highlights how increased molecular complexity can yield complex structures even if they are not equilibrium. This is further shown by the successful inverse design (although not negative selection) of untapered triblock copolymers to yield viable target microstructures. Examination of the trajectories taken during negative selection indicate that for the triblock case, tapering offers only modest to little additional benefit in bringing the desired microstructures into closer metastable contention (*SI Appendix*). This indicates that additional sequence complexity—either via tapering or an additional block—is necessary to achieve more complex microstructure designs.

While this demonstration was unable to yield a simple linearly tapered block to achieve one of the complex Frank-Kasper morphologies as the equilibrium structure, it demonstrates that increasing sequence complexity does offer additional design levers. Only a simple example of sequence control was tested here. With this work's inverse design algorithm, any differentiable sequence function representation can be tested. Different functional classes such as sinusoidal waves or Chebyshev basis functions can be explored to impart more complex nonlinear tapers into the sequence design. The power of the inverse design algorithm to rapidly screen large regions of the sequence design landscape motivates the development of more flexible copolymer representations which allow access to more of the design landscape. Even if no sequence is designed which yields the desired microstructure as the equilibrium, this knowledge is still valuable in preventing costly computational or experimental searches in unpromising design.

Identifying the Minimum Number of Blocks for Achieving Complex Morphologies. The power of the inverse design and negative selection algorithms was demonstrated by navigating the massive multiblock design space to find the minimum number of blocks required to stabilize several complex morphologies. This addresses the question posed by Bates et al., of whether the multiblock landscape is a panacea opening the door to a host of new phases, or a Pandora's box where the wealth of possible designs hinders discovery of new sequences (61). Fundamentally, it demonstrates the power of the algorithm to seek minimally complex solutions to specified design challenges.

In linear, conformationally symmetric block copolymers, two sets of parameters, the block fractions f and the interblock interaction potentials χN, control the phase diagram of equilibrium microstructures (86). The resulting self-assembled structures are describable by symmetries belonging to one of the 230 crystallographic space groups (29). For a diblock copolymer, SCFT predicts structures belonging to six distinct space groups, of which five have been experimentally observed (30, 87, 88). In triblock phase diagrams, structures in these five space groups continue to dominate, with only two new space groups observed with limited regions of stability (89–91). However, recent experiments have shown that an array of complex sphere-forming Frank-Kasper phases in additional space groups can be formed in diblocks with block conformational asymmetry (50, 82, 92, 93). This motivates the question of whether block number alone can be used as a design lever to generate complex microstructures. This question has been difficult to answer due to the combinatorial explosion of sequence possibilities to consider with each additional block, where Bates et al. calculated over 27 million block permutations for a decablock, with a near infinite number of additional χN and block fraction possibilities (61).

Here, the inverse design algorithm was used to answer this question. Block copolymers were inverse designed to form a target structure belonging to 16 space groups not common or not previously achieved in linear block copolymer systems. Only the block number was specified a priori, while all other molecular details such as block fraction and interblock χN potential were optimized via the inverse design algorithm. For inverse designed sequences, the second part of the algorithm—negative selection—was performed to bring the target structure into equilibrium against competing structures in the 5 commonly observed space groups ($P\overline{1}$, $p6mm$, $Ia\overline{3}d$, $Im\overline{3}m$, and $Fddd$).

Out of the 16 space groups, only 1 was not successfully designed to be the stable equilibrium among considered candidates (Fig. 4). While the minimal number of blocks required varied, the results reveal that increasing block number does open the door to more complex morphological designs. Table 1 reports the minimum number of blocks for the sequence design which successfully brings the target space group into equilibrium. The closest alternate candidate phase along with the difference in free energy to this phase is also reported. The block fractions and interblock χN for the designed multiblocks are provided in *SI Appendix*.

The spatial distribution of blocks combined with the interblock χN reveal how a multiblock stabilizes complex morphologies. The first is a single gyroid structure found in the $I2_13$ space group. The $I2_13$ space group is a lower symmetry variant of the $I4_132$ space group of which single gyroid structures have previously been reported for multiblock copolymers including triblocks (89, 94, 95). Unlike the results of Tyler et al., the triblock design here has strong interaction penalty between the A-B and B-C blocks and a weaker A-C interaction penalty ($\chi_{AB}N = 24.15,\ \ \chi_{AC}N = 14.22,\ \ \chi_{BC}N = 26.45$) (89). As shown in Fig. 5*B*, for the single gyroid the A block remains relatively diffuse throughout the domain, with its maximal volume fraction near its block fraction of 0.22. Together, the A and B blocks form one half of the gyroid structure, while the C block forms the other half. The closest competing alternate structure is a hexagonal cylinder with $p6mm$ symmetry. Unlike the gyroid, the cylindrical structure is composed of three distinct layers with the A domain concentrated in the core of the cylinder, the B domain forming the shell, and the C domain filling the space between cylinders. From these observations, it can be hypothesized that one contributor to the single gyroid stability could be the more diffuse A domain, resulting in less chain stretching in the gyroid than the cylindrical

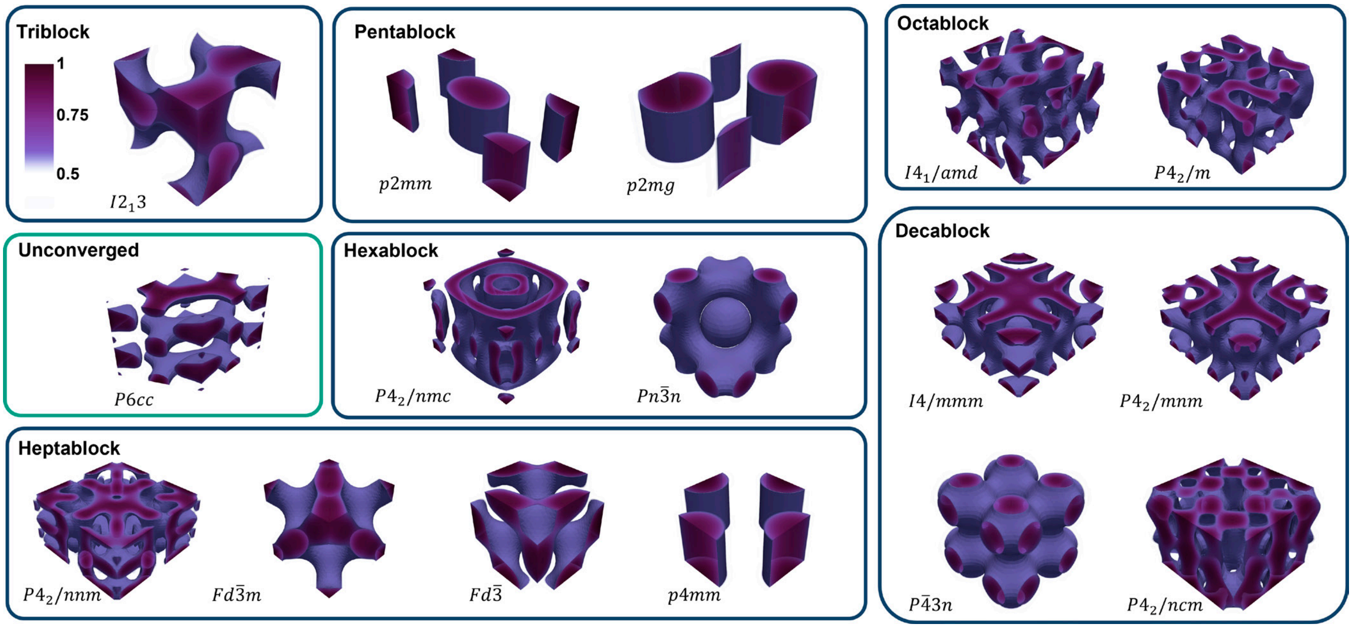

Fig. 4. Several complex structures in previously unobserved space groups were inverse designed and negatively selected against structures belonging to the five classical diblock copolymer space groups. Structures are categorized according to the number of blocks necessary to achieve a successful negative selection among considered alternates.

configuration. The symmetry of the cylindrical structure means that there is no A-C interface due to the placement of the B domain, despite the lower $\chi_{AC}N$. In the single gyroid configuration, the existence of a weak A-C interface is expected to contribute little to the interaction energy penalty but might result in more favorable single chain configurations. This hypothesis is supported by the fact that higher multiblock structures which successfully inverse design and negatively select for the single gyroid $I2_13$ structure share a similar sequence motif with a large middle block with strong interaction penalty with the ends. Two multiblock designs (octablock and decablock) which did not successfully negatively select for the single gyroid do not possess these features (Fig. 5*C*, additional sequences and their interaction matrices in *SI Appendix*). It is probable that for these designs, the initial guess and inverse design led to a metastable 'trapped' state where the small sequence changes of the negative selection step were unable to bring the sequence into an equilibrium design.

Table 1. Multiblocks form stable novel structures

Space group	Minimum block #	$\lvert\Delta F/nk_bT\rvert$ to closest alternate structure	Closest alternate space group
$P6cc$	– (Up to 10)	–	–
$I2_13$	3	0.01350	$p6mm$
$p2mm$	5	0.00013	$p6mm$
$p2mg$	5	0.00002	$p6mm$
$P4_2/nmc$	6	0.00207	$Ia\bar{3}d$
$Pn\bar{3}n$	6	0.00406	$P\bar{1}$
$P4_2/nnm$	7	0.00555	$Ia\bar{3}d$
$Fd\bar{3}m$	7	0.29365	$Fddd$
$Fd\bar{3}$	7	0.00348	$Ia\bar{3}d$
$p4mm$	7	0.00030	$p6mm$
$I4_1/amd$	8	0.00571	$Im\bar{3}m$
$P4_2/m$	8	0.28692	$Im\bar{3}m$
$I4/mmm$	10	0.00690	$P\bar{1}$
$P4_2/mnm$	10	0.00132	$P\bar{1}$
$P\bar{4}3n$	10	0.00297	$Ia\bar{3}d$
$P4_2/ncm$	10	0.01421	$Ia\bar{3}d$

Another interesting structure is the formation of a bicontinuous cubic network in the $P\bar{4}3n$ space group. The formed structure resembles that of the primitive surface structure commonly observed in aqueous lipid solutions (96). The primitive surface is not preferred in copolymer melts due to packing frustration of the polymer at the sixfold connection; instead, the fourfold connection of the double diamond or double gyroid surface is the preferred stable structure (97–99). Until recently, the only accessible route for these structures in neat diblock melts has been via careful processing to trap the copolymer in a metastable state (98). A recent work by Lee et al. successfully accessed the primitive network in a diblock as the equilibrium structure through modulation of the packing and attraction of the endgroups to stabilize the sixfold connector (99). Can the primitive network be accessed in a multiblock by solely tuning the interblock potential and block fraction? The results here hint that a network with the primitive surface is formable, but without the full symmetries of the $Im\bar{3}m$ space group. Strikingly, 10 blocks were required to stabilize this phase with lower free energy than the compared structures, one of which is the double gyroid in the $Ia\bar{3}d$ space group. Fig. 5*D* illustrates the designed decablock sequence, which exhibits a few extremely interblock χN especially with Block IV. The plotted structure is an amalgamation of blocks III, IV, V, VII, VIII, and IX; therefore, the spatial distribution of Block IV especially with respect to its unfavorable interaction partners must play a role in stabilizing the sixfold connector. Fig. 5*E* shows the packing of several of these interaction partners and Block IV. Block IV forms the interior of the primitive surface, and heuristically, the highly unfavorable interactions between it and its flanking Block II and Block VI could be one source of stabilization against the

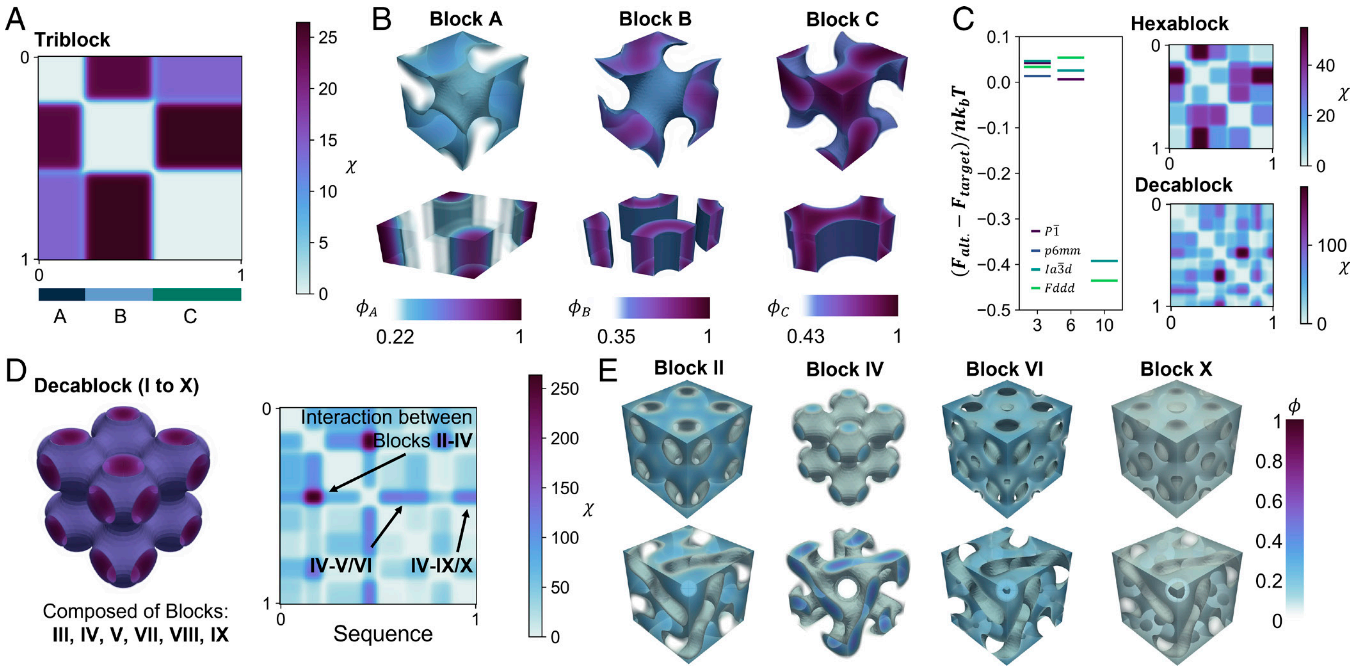

Fig. 5. Increased sequence complexity via block number allows complex microstructures to be accessed. (*A*–*C*) The single gyroid structure in the $I2_13$ space group is examined. (*A*) the sequence function is a triblock and the resulting interaction matrix is shown. (*B*) The spatial distribution of each block for the single gyroid and the closest competing structure (hexagonal cylinder) is shown. (*C*) The free energy difference between alternate microstructures and the target is shown for negatively selected triblock, hexablock, and decablock designs. For the triblock and hexablock, there is a conserved sequence motif which is the midblock with strong interaction repulsion with the endblocks. For the designed decablock, this motif was not present. (*D* and *E*) An analysis on the $P\bar{4}3n$ structure designed for by the decablock is shown. (*D*) Block IV was identified as having a high χN interaction with several blocks. (*E*) The spatial distribution of these other blocks with block IV indicate how this energetically unfavorable interaction could be the origin of stabilizing the tightly packed sixfold junction over the less packed gyroid structure junction.

unfavorable chain stretching and packing frustration experienced in the sixfold junction (97, 100). However, the closest alternate gyroid-like structure in the $Ia\bar{3}d$ space group similarly displays segregation between Block IV and Blocks II, VI, and X. Further analysis of the inverse designed sequences especially for complex multiblocks is required to fully understand the origins of stability for these unexpected structures.

A few limitations of the current inverse design and negative selection workflow merit discussion. First, the success or failure of inverse design is highly dependent on the target structure. Even if during negative selection, the target structure is not enforced and instead any structure in the target space group is selected for, the initial inverse design toward an unsuitable target can "trap" the algorithm in an unsuitable location in the sequence design space. This is evident in the failure of the octablock and decablock multiblock to converge an equilibrium single gyroid as described earlier.

Another surprising result was the inability to design a square cylinder structure in the *p*4*mm* space group with fewer than 7 blocks, given that other studies have reported the existence of cylinders with *p*4*mm* symmetry in linear multiblocks with tetrablock and pentablock copolymers (101, 102). There may be several reasons for the higher number of blocks required here. First, the initial inverse designed target is extremely important. Unlike other studies, the targeted structure formed by the *p*4*mm* space group are cylinders at the faces between unit cells, rather than at the edges which alters the resulting symmetries. This highlights the importance of target selection, especially since a single space group can contain many structures including metastable ones. Second, analysis of the designed heptablock sequence (*SI Appendix*) reveals that two of the blocks (4, 5) contribute together less than 0.05 of the block fraction and have similar interblock χN as block 6. If these are merged with block 6, then the resulting block copolymer sequence is a pentablock. This highlights another limitation, where the sequence with a lower number of blocks might not negatively select for the desired structure in the specified number of iterations.

A second limitation is the number of alternate structures considered during negative selection. Here, only five alternate space groups were considered with two candidate structures in each (10 total structures considered). A more complete negative selection should include not only other space groups, but multiple candidate structures in these space groups; however, given limited knowledge of what alternate structures are formable for these multiblock sequences, this is a difficult task. Without such a full negative selection, the results presented here represent only an equilibrium among considered alternates and might not be the true equilibrium. One solution in generating better alternate structures for sampling in negative selection is the incorporation of phase discovery algorithms such as the recently developed GAN algorithm of Chen and Dorfman (103), or other discovery methods using genetic, Bayesian, or neural network algorithms (54, 104, 105). Despite these limitations, the results presented here represent a significant leap in capabilities and offers a glimpse of the more rapid microstructure discovery workflow that can be achieved with a robust inverse design algorithm.

Beyond Melts: Inverse Designing Micelles in Polymer Solutions. SCFT offers a robust thermodynamic model not just for block copolymer melts but for a wide range of soft matter systems. Many of these systems are of high scientific and engineering interest; these include block copolymers in the presence of external forces such as electric fields (106) or shear (107), polyelectrolytes (108–111), architecturally complex copolymers (i.e. star, H, ring, etc.) (112–115), liquid crystalline polymers (116, 117), amphiphilic copolymer solutions (118, 119), and even biological membranes (120). The inverse design algorithm presented in this work is extendable to any polymer system for which SCFT provides an accurate thermodynamic model of self-assembly. To demonstrate this capability, inverse design was demonstrated on copolymer micelles using the SCFT model presented in Cai et al. (119) A micelle structure with $Pm\bar{3}m$ space group symmetry was set as the target in a polymer solution with 10% polymer fraction. The inverse design algorithm learned an amphiphilic copolymer sequence which generated the targeted micelle. The learned copolymer is a near symmetric diblock where the block (A) forming the core of the micelle has Flory–Huggins interaction parameter with the solvent (S) $\chi_{AS} = 0.286$, the corona block (B) has $\chi_{BS} = 12.302$, while the interblock interaction strength is $\chi_{AB}N = 16.30$ (see *SI Appendix* for more details). This example illustrates this work's potential for generality in achieving inverse design across soft matter, moving the community one step closer to programmable materials.

Conclusion

Molecular-level programming of structure-dependent material properties requires designing molecules that can self-assemble into target structures. Copolymer melts represent a compelling system for demonstrating the power of inverse design algorithms to perform this design calculation due to the diversity of potential microstructures, the intractably large sequence design landscape, and the existence of a robust thermodynamics model in SCFT. In this work, the inverse design challenge was met with an algorithm which directly learns the self-assembly language of copolymers via an SCFT adjoint solution. This approach drives the sequence design across the design landscape toward a viable solution and does not require that the solution is interpolated among sampled points. Validation of this approach was conducted by demonstrating the successful design of a diblock sequence to the small stability window of the O^{70} network phase starting from an arbitrary sequence deep in the disordered region.

As a demonstration of the power of this approach, two long-standing questions in copolymer physics have been addressed. First, the power of sequence-controlled copolymers to enable complex microstructures was explored through the incorporation of simple linear tapering in diblock and triblock copolymers. While negative selection showed that a sequence yielding equilibrium Frank-Kasper phases could not be found for the simple sequence control considered here, inverse design yielded metastable sequence designs which represent possible targets for processing-controlled self-assembly. Second, the multiblock design landscape was traversed in search of the minimally complex copolymer sequence which can produce a novel target microstructure. Several microstructures containing space group symmetries previously unreported in block copolymers were designed to be the equilibrium morphology. The convergence to a minimally complex solution is one criterion of the inverse design challenge and fulfilled by this algorithm. The power of inverse design to navigate through the entire design landscape in search of sequence which achieve challenging design targets is aptly demonstrated with these examples. Nevertheless, the inverse design challenge is not fully resolved. Experimentally realizing the sequences produced here which require a precise and sequence-controlled series of χN values with real copolymers is expected to be a challenge. Advances in chemical synthesis to achieve a greater range of χ values via a greater palette of monomers, postpolymerization modifications, end-group modulation, and statistical blending of monomers all hold promise in achieving polymers with the necessary complexity (99, 121–128). In addition, the full potential of inverse design can only be exploited with a structure discovery algorithm which supplies valid design targets and alternate structures necessary for negative selection. Recent advances such as the GAN structure discovery algorithm by Chen and Dorfman show promise as a robust structure discovery algorithm (103).

With SCFT as the theoretical foundations, the possibilities of extending inverse design for copolymer melts to include other design levers on microstructure formation such as external electric potential field (106), electrostatic effects for polyelectrolytes (108–111), shear-induced phase formation (107), as well as other block copolymer architectures (112–114) are large. As a demonstration of this potential, the inverse design algorithm was extended to polymer solution micelles. Copolymer melts share the essential physics present across self-assembling soft matter systems. In addition, the two questions addressed here represent the search for minimally complex molecular features which yield a desired self-assembled structure, a task which is foundational across soft matter. The demonstration of robust inverse design in this work holds promise to generalize across many other systems and is key step toward precise engineering of tailored soft materials.

Data, Materials, and Software Availability. The inverse design algorithm with negative selection can be accessed at https://github.com/olsenlabmit/scft-id (129). In the same repository, analysis code is provided for generating the plots shown in this text and for performing other analysis. Data for the O70 and micelle diblock design are available in the repository. The data for all structures designed in this text are available at https://doi.org/10.5281/zenodo.15756493 (130). The results of inverse design and negative selection for the structures shown in text can be accessed here https://doi.org/10.5281/zenodo.15756753 (131) and can be analyzed using the provided code.

ACKNOWLEDGMENTS. This work was supported by the Department of Energy through the Basic Energy Sciences program (Award DE-SC000710). We acknowledge the MIT Office of Research Computing and Data for providing high-performance computing resources that have contributed to the research results reported within this paper. A.E.C. would like to acknowledge funding through the National Defense Science and Engineering Graduate Fellowship.

1. A. M. C. Emons, B. M. Mulder, The making of the architecture of the plant cell wall: How cells exploit geometry. *Proc. Natl. Acad. Sci. U.S.A.* **95**, 7215–7219 (1998).
2. A. N. Fernandes *et al.*, Nanostructure of cellulose microfibrils in spruce wood. *Proc. Natl. Acad. Sci. U.S.A.* **108**, E1195–E1203 (2011).
3. S. Li *et al.*, Cellulose synthase complexes act in a concerted fashion to synthesize highly aggregated cellulose in secondary cell walls of plants. *Proc. Natl. Acad. Sci. U.S.A.* **113**, 11348–11353 (2016).
4. B. Winter *et al.*, Coexistence of both gyroid chiralities in individual butterfly wing scales of Callophrys rubi. *Proc. Natl. Acad. Sci. U.S.A.* **112**, 12911–12916 (2015).
5. V. Saranathan, S. Narayanan, A. Sandy, E. R. Dufresne, R. O. Prum, Evolution of single gyroid photonic crystals in bird feathers. *Proc. Natl. Acad. Sci. U.S.A.* **118**, e2101357118 (2021).
6. V. Saranathan *et al.*, Structure, function, and self-assembly of single network gyroid (14_132) photonic crystals in butterfly wing scales. *Proc. Natl. Acad. Sci. U.S.A.* **107**, 11676–11681 (2010).
7. P. Vukusic, J. R. Sambles, Photonic structures in biology. *Nature* **424**, 852–855 (2003).
8. J. R. Espinosa *et al.*, Liquid network connectivity regulates the stability and composition of biomolecular condensates with many components. *Proc. Natl. Acad. Sci. U.S.A.* **117**, 13238–13247 (2020).
9. S. T. Arold, P. G. Leonard, G. N. Parkinson, J. E. Ladbury, H-NS forms a superhelical protein scaffold for DNA condensation. *Proc. Natl. Acad. Sci. U.S.A.* **107**, 15728–15732 (2010).
10. A. L. Turner *et al.*, Highly disordered histone H1−DNA model complexes and their condensates. *Proc. Natl. Acad. Sci. U.S.A.* **115**, 11964–11969 (2018).
11. R. Renger *et al.*, Co-condensation of proteins with single- and double-stranded DNA. *Proc. Natl. Acad. Sci. U.S.A.* **119**, e2107871119 (2022).
12. M. Feric *et al.*, Mesoscale structure–function relationships in mitochondrial transcriptional condensates. *Proc. Natl. Acad. Sci. U.S.A.* **119**, e2207303119 (2022).
13. N. Vogel *et al.*, Color from hierarchy: Diverse optical properties of micron-sized spherical colloidal assemblies. *Proc. Natl. Acad. Sci. U.S.A.* **112**, 10845–10850 (2015).
14. X. Zhao, Designing toughness and strength for soft materials. *Proc. Natl. Acad. Sci. U.S.A.* **114**, 8138–8140 (2017).
15. J. P. Gong, Materials both tough and soft. *Science* **344**, 161–162 (2014).
16. C. Huang, D. Quinn, S. Suresh, K. J. Hsia, Controlled molecular self-assembly of complex three-dimensional structures in soft materials. *Proc. Natl. Acad. Sci. U.S.A.* **115**, 70–74 (2018).
17. P. P. Ghoroghchian *et al.*, Near-infrared-emissive polymersomes: Self-assembled soft matter for in vivo optical imaging. *Proc. Natl. Acad. Sci. U.S.A.* **102**, 2922–2927 (2005).
18. E. Winfree, F. Liu, L. A. Wenzler, N. C. Seeman, Design and self-assembly of two-dimensional DNA crystals. *Nature* **394**, 539–544 (1998).

19. E. Munch *et al.*, Tough, bio-inspired hybrid materials. *Science* **322**, 1516–1520 (2008).
20. G. M. Coli, E. Boattini, L. Filion, M. Dijkstra, Inverse design of soft materials via a deep learning–based evolutionary strategy. *Sci. Adv.* **8**, eabj6731 (2022).
21. J. N. Kumar *et al.*, Machine learning enables polymer cloud-point engineering via inverse design. *NPJ Comput. Mater.* **5**, 73 (2019).
22. H. M. Jaeger, J. J. Pablo, Perspective: Evolutionary design of granular media and block copolymer patterns. *APL Mater.* **4**, 053209 (2016).
23. V. Liao, A. Jayaraman, Inverse design of block polymer materials with desired nanoscale structure and macroscale properties. *JACS Au* **5**, 2810–2824 (2025).
24. K. Hiraide, K. Hirayama, K. Endo, M. Muramatsu, Application of deep learning to inverse design of phase separation structure in polymer alloy. *Comput. Mater. Sci.* **190**, 110278 (2021).
25. A. Z. Nelson, R. H. Ewoldt, Design of yield-stress fluids: A rheology-to-structure inverse problem. *Soft Matter* **13**, 7578–7594 (2017).
26. Y. Zheng *et al.*, AI-guided inverse design and discovery of recyclable vitrimeric polymers. *Adv. Sci.* **12**, 2411385 (2025).
27. E. L. Thomas, The ABCs of self-assembly. *Science* **286**, 1307–1307 (1999).
28. F. S. Bates, G. H. Fredrickson, Block copolymers—Designer soft materials. *Phys. Today* **52**, 32–38 (1999).
29. I. W. Hamley, *The Physics of Block Copolymers* (Oxford University Press, Oxford, 1998).
30. F. S. Bates, G. H. Fredrickson, Block copolymer thermodynamics: Theory and experiment. *Annu. Rev. Phys. Chem.* **41**, 525–557 (1990).
31. C. M. Bates, F. S. Bates, 50th anniversary perspective: Block polymers—Pure potential. *Macromolecules* **50**, 3–22 (2017).
32. J.-F. Lutz, M. Ouchi, D. R. Liu, M. Sawamoto, Sequence-controlled polymers. *Science* **341**, 1238149 (2013).
33. A. Zunger, Inverse design in search of materials with target functionalities. *Nat. Rev. Chem.* **2**, 0121 (2018).
34. B. Y. J. Wong, M. Damodaran, B. C. Khoo, Physics-informed machine learning using low-fidelity flowfields for inverse airfoil shape design. *AIAA J.* **62**, 1–16 (2024), 10.2514/1.J063570.
35. S. Colburn, A. Majumdar, Inverse design and flexible parameterization of meta-optics using algorithmic differentiation. *Commun. Phys.* **4**, 65 (2021).
36. V. Liao, T. Myers, A. Jayaraman, A computational method for rapid analysis polymer structure and inverse design strategy (RAPSIDY). *Soft Matter* **20**, 8246–8259 (2024).
37. T. K. Patra, T. D. Loeffler, S. K. R. S. Sankaranarayanan, Accelerating copolymer inverse design using monte carlo tree search. *Nanoscale* **12**, 23653–23662 (2020).
38. E. Helfand, Theory of inhomogeneous polymers: Fundamentals of the Gaussian random-walk model. *J. Chem. Phys.* **62**, 999–1005 (1975).
39. E. Helfand, Block copolymer theory. III. Statistical mechanics of the microdomain structure. *Macromolecules* **8**, 552–556 (1975).
40. M. W. Matsen, M. Schick, Stable and unstable phases of a diblock copolymer melt. *Phys. Rev. Lett.* **72**, 2660–2663 (1994).
41. P. Stasiak, M. W. Matsen, Efficiency of pseudo-spectral algorithms with Anderson mixing for the SCFT of periodic block-copolymer phases. *Eur. Phys. J. E* **34**, 110 (2011).
42. M. W. Matsen, Fast and accurate SCFT calculations for periodic block-copolymer morphologies using the spectral method with Anderson mixing. *Eur. Phys. J. E* **30**, 361 (2009).
43. C. A. Tyler, D. C. Morse, Stress in self-consistent-field theory. *Macromolecules* **36**, 8184–8188 (2003).
44. A. Arora, D. C. Morse, F. S. Bates, K. D. Dorfman, Accelerating self-consistent field theory of block polymers in a variable unit cell. *J. Chem. Phys.* **146**, 244902 (2017).
45. A. Arora *et al.*, Broadly accessible self-consistent field theory for block polymer materials discovery. *Macromolecules* **49**, 4675–4690 (2016).
46. G. H. Fredrickson, *The Equilibrium Theory of Inhomogeneous Polymers* (Clarendon Press, Oxford, 2006).
47. K. Ø. Rasmussen, G. Kalosakas, Improved numerical algorithm for exploring block copolymer mesophases. *J. Polym. Sci. B Polym. Phys.* **40**, 1777–1783 (2002).
48. E. W. Cochran, C. J. Garcia-Cervera, G. H. Fredrickson, Stability of the gyroid phase in diblock copolymers at strong segregation. *Macromolecules* **39**, 2449–2451 (2006).
49. M. W. Matsen, Gyroid versus double-diamond in ABC triblock copolymer melts. *J. Chem. Phys.* **108**, 785–796 (1998).
50. M. W. Bates *et al.*, Stability of the A15 phase in diblock copolymer melts. *Proc. Natl. Acad. Sci. U.S.A.* **116**, 13194–13199 (2019).
51. D. A. Hajduk *et al.*, Stability of the perforated layer (PL) phase in diblock copolymer melts. *Macromolecules* **30**, 3788–3795 (1997).
52. M. R. Khadilkar, S. Paradiso, K. T. Delaney, G. H. Fredrickson, Inverse design of bulk morphologies in multiblock polymers using particle swarm optimization. *Macromolecules* **50**, 6702–6709 (2017).
53. L. J. Case, K. T. Delaney, G. H. Fredrickson, F. S. Bates, K. D. Dorfman, Open-source platform for block polymer formulation design using particle swarm optimization. *Eur. Phys. J. E* **44**, 115 (2021).
54. C. L. Tsai, G. H. Fredrickson, Using particle swarm optimization and self-consistent field theory to discover globally stable morphologies of block copolymers. *Macromolecules* **55**, 5249–5262 (2022).
55. Q. Dong *et al.*, Inverse design of complex block copolymers for exotic self-assembled structures based on Bayesian optimization. *ACS Macro Lett.* **12**, 401–407 (2023).
56. J. Qin *et al.*, Evolutionary pattern design for copolymer directed self-assembly. *Soft Matter* **9**, 11467 (2013).
57. G. S. Khaira *et al.*, Evolutionary optimization of directed self-assembly of triblock copolymers on chemically patterned substrates. *ACS Macro Lett.* **3**, 747–752 (2014).
58. A. F. Hannon, K. W. Gotrik, C. A. Ross, A. Alexander-Katz, Inverse design of topographical templates for directed self-assembly of block copolymers. *ACS Macro Lett.* **2**, 251–255 (2013).
59. D. Lin, H. Y. Yu, Deep learning and inverse discovery of polymer self-consistent field theory inspired by physics-informed neural networks. *Phys. Rev. E* **106**, 014503 (2022).
60. H. Wang, S. Li, J. Zeng, T. Zhang, Accelerating polymer self-consistent field simulation and inverse DSA-lithography with deep neural networks. *J. Chem. Phys.* **162**, 104105 (2025).
61. F. S. Bates *et al.*, Multiblock polymers: Panacea or Pandora's box? *Science* **336**, 434–440 (2012).
62. O. Xie, B. D. Olsen, A self-consistent field theory formalism for sequence-defined polymers. *Macromolecules* **55**, 6516–6524 (2022).
63. A. F. M. Barton, *CRC Handbook of Solubility Parameters and Other Cohesion Parameters* (CRC Press, Boca Raton, 1991).
64. Y. Qiang, W. Li, Accelerated pseudo-spectral method of self-consistent field theory via crystallographic fast Fourier transform. *Macromolecules* **53**, 9943–9952 (2020).
65. S. Molesky *et al.*, Inverse design in nanophotonics. *Nat. Photonics* **12**, 659–670 (2018).
66. S. P. Paradiso, K. T. Delaney, G. H. Fredrickson, Swarm intelligence platform for multiblock polymer inverse formulation design. *ACS Macro Lett.* **5**, 972–976 (2016).
67. M. Ye, B. Liu, S. Wright, P. Stone, Q. Liu, BOME! Bilevel optimization made easy: A simple first-order approach. arXiv [Preprint] (2022). https://arxiv.org/abs/2209.08709 (Accessed 25 April 2025).
68. C. A. Tyler, D. C. Morse, Orthorhombic Fddd network in triblock and diblock copolymer melts. *Phys. Rev. Lett.* **94**, 208302 (2005).
69. M. W. Matsen, Effect of architecture on the phase behavior of AB-type block copolymer melts. *Macromolecules* **45**, 2161–2165 (2012).
70. S. L. Perry, C. E. Sing, 100th anniversary of macromolecular science viewpoint: Opportunities in the physics of sequence-defined polymers. *ACS Macro Lett.* **9**, 216–225 (2020), 10.1021/acsmacrolett.0c00002.
71. A. J. DeStefano, R. A. Segalman, E. C. Davidson, Where biology and traditional polymers meet: The potential of associating sequence-defined polymers for materials science. *JACS Au* **1**, 1556–1571 (2021).
72. W. F. Reinhart, A. Statt, Opportunities and challenges for inverse design of nanostructures with sequence defined macromolecules. *Acc. Mater. Res.* **2**, 697–700 (2021), 10.1021/accountsmr.1c00089.
73. R. Roy *et al.*, Double-gyroid network morphology in tapered diblock copolymers. *Macromolecules* **44**, 3910–3915 (2011).
74. J. R. Brown, S. W. Sides, L. M. Hall, Phase behavior of tapered diblock copolymers from self-consistent field theory. *ACS Macro Lett.* **2**, 1105–1109 (2013).
75. K. Kim *et al.*, Thermal processing of diblock copolymer melts mimics metallurgy. *Science* **356**, 520–523 (2017).
76. S. Chanpuriya *et al.*, Cornucopia of nanoscale ordered phases in sphere-forming tetrablock terpolymers. *ACS Nano* **10**, 4961–4972 (2016).
77. J. Lee, D. Kim, Large-scale 3D fast Fourier transform computation on a GPU. *ETRI J.* **45**, 1035–1045 (2023).
78. S. A. Aseeri, "Distributed memory fast fourier transforms in the exascale era" in *2025 International Conference on Intelligent Control, Computing and Communications (IC3)* (IEEE, 2025), pp. 1043–1046, 10.1109/IC363308.2025.10956891.
79. Y. Chen, X. Cui, H. Mei, "Large-scale FFT on GPU clusters" in *Proceedings of the 24th ACM International Conference on Supercomputing* (ACM, New York, NY, 2010), pp. 315–324, 10.1145/1810085.1810128.
80. N. Xie, W. Li, F. Qiu, A.-C. Shi, σ phase formed in conformationally asymmetric AB-type block copolymers. *ACS Macro Lett.* **3**, 906–910 (2014).
81. H. Lee, J. Kim, M. J. Park, Exploration of complex nanostructures in block copolymers. *Phys. Rev. Mater.* **8**, 020302 (2024).
82. A. Reddy *et al.*, Stable Frank-Kasper phases of self-assembled, soft matter spheres. *Proc. Natl. Acad. Sci. U.S.A.* **115**, 10233–10238 (2018).
83. X.-J. Geng *et al.*, Process-directed self-assembly of the Frank-Kasper A15 structure in linear, conformationally symmetric block copolymers. *Phys. Rev. Lett.* **134**, 118102 (2025).
84. C.-Y. Chang, Y.-H. Chen, R.-M. Ho, Metastable network phases from controlled self-assembly of high-χ block copolymers. *Phys. Rev. Mater.* **8**, 030301 (2024).
85. D.-W. Sun, M. Müller, Process-accessible states of block copolymers. *Phys. Rev. Lett.* **118**, 067801 (2017).
86. F. S. Bates, Polymer-polymer phase behavior. *Science* **251**, 898–905 (1991).
87. M. Takenaka *et al.*, Orthorhombic Fddd network in diblock copolymer melts. *Macromolecules* **40**, 4399–4402 (2007).
88. M. F. Schulz *et al.*, Phase behavior of polystyrene—poly(2-vinylpyridine) diblock copolymers. *Macromolecules* **29**, 2857–2867 (1996).
89. C. A. Tyler, J. Qin, F. S. Bates, D. C. Morse, SCFT study of nonfrustrated ABC triblock copolymer melts. *Macromolecules* **40**, 4654–4668 (2007).
90. W. Zheng, Z.-G. Wang, Morphology of ABC triblock copolymers. *Macromolecules* **28**, 7215–7223 (1995).
91. T. H. Epps *et al.*, Ordered network phases in linear poly(isoprene-b-styrene-b-ethylene oxide) triblock copolymers. *Macromolecules* **37**, 8325–8341 (2004).
92. S. Lee, C. Leighton, F. S. Bates, Sphericity and symmetry breaking in the formation of Frank-Kasper phases from one component materials. *Proc. Natl. Acad. Sci. U.S.A.* **111**, 17723–17731 (2014).
93. S. Lee, M. J. Bluemle, F. S. Bates, Discovery of a Frank-Kasper σ phase in sphere-forming block copolymer melts. *Science* **330**, 349–353 (2010).
94. H.-F. Wang *et al.*, Networks with controlled chirality via self-assembly of chiral triblock terpolymers. *Sci. Adv.* **6**, eabc3644 (2020).
95. Q. Xie, Y. Qiang, W. Li, Single gyroid self-assembled by linear BABAB pentablock copolymer. *ACS Macro Lett.* **11**, 205–209 (2022).
96. T. Oka, Transformation between inverse bicontinuous cubic phases of a lipid from diamond to primitive. *Langmuir* **31**, 3180–3185 (2015).
97. A. Reddy, M. S. Dimitriyev, G. M. Grason, Medial packing and elastic asymmetry stabilize the double-gyroid in block copolymers. *Nat. Commun.* **13**, 2629 (2022).
98. C.-Y. Chang *et al.*, Mesoscale networks and corresponding transitions from self-assembly of block copolymers. *Proc. Natl. Acad. Sci. U.S.A.* **118**, e2022275118 (2021).
99. H. Lee *et al.*, Thermodynamically stable plumber's nightmare structures in block copolymers. *Science* **383**, 70–76 (2024).
100. M. S. Dimitriyev, A. Reddy, G. M. Grason, Medial packing, frustration, and competing network phases in strongly segregated block copolymers. *Macromolecules* **56**, 7184–7202 (2023).
101. K. Yuan, Z. Xu, X. Huang, W. Li, Reexamining the emergence and stability of the square cylinder phase in block copolymers. *Chem. A Eur. J.* **29**, e202301043 (2023).
102. H. Yoon, Q. Dong, W. Li, J. K. Kim, Tetragonally and rectangularly packed hierarchical cylinders from A_1BA_2C tetrablock terpolymer. *Macromol. Rapid Commun.* **46**, 2300312 (2025).
103. P. Chen, K. D. Dorfman, Gaming self-consistent field theory: Generative block polymer phase discovery. *Proc. Natl. Acad. Sci. U.S.A.* **120**, e2308698120 (2023).
104. Y. Xuan, K. T. Delaney, H. D. Ceniceros, G. H. Fredrickson, Deep learning and self-consistent field theory: A path towards accelerating polymer phase discovery. *J. Comput. Phys.* **443**, 110519 (2021).
105. Q. Dong *et al.*, Automated search strategy for novel ordered structures of block copolymers. *ACS Macro Lett.* **13**, 987–993 (2024).

106. J. M. Martin, W. Li, K. T. Delaney, G. H. Fredrickson, SCFT study of diblock copolymer melts in electric fields: Selective stabilization of orthorhombic Fddd network phase. *Macromolecules* **51**, 3369–3378 (2018).
107. D.-W. Sun, M. Müller, Step-shear deformation of block copolymers. *Macromolecules* **51**, 8386–8405 (2018).
108. C. E. Sing, S. L. Perry, Recent progress in the science of complex coacervation. *Soft Matter* **16**, 2885–2914 (2020).
109. T. K. Lytle, C. E. Sing, Transfer matrix theory of polymer complex coacervation. *Soft Matter* **13**, 7001–7012 (2017).
110. T. K. Lytle, L.-W. Chang, N. Markiewicz, S. L. Perry, C. E. Sing, Designing electrostatic interactions via polyelectrolyte monomer sequence. *ACS Cent. Sci.* **5**, 709–718 (2019).
111. C. E. Sing, J. W. Zwanikken, M. O. Cruz, Theory of melt polyelectrolyte blends and block copolymers: Phase behavior, surface tension, and microphase periodicity. *J. Chem. Phys.* **142**, 034902 (2015).
112. M. W. Matsen, F. S. Bates, Conformationally asymmetric block copolymers. *J. Polym. Sci. Part B: Polym. Phys.* **35**, 945 (1997).
113. S. J. Park, G. K. Cheong, F. S. Bates, K. D. Dorfman, Stability of the double gyroid phase in bottlebrush diblock copolymer melts. *Macromolecules* **54**, 9063–9070 (2021).
114. G. Zhang, F. Qiu, H. Zhang, Y. Yang, A.-C. Shi, SCFT study of tiling patterns in ABC star terpolymers. *Macromolecules* **43**, 2981–2989 (2010).
115. Y. Qiang, W. Li, Accelerated method of self-consistent field theory for the study of Gaussian ring-type block copolymers. *Macromolecules* **54**, 9071–9078 (2021).
116. W. Song, P. Tang, F. Qiu, Y. Yang, A.-C. Shi, Phase behavior of semiflexible-coil diblock copolymers: A hybrid numerical SCFT approach. *Soft Matter* **7**, 929–938 (2011).
117. D. Wei, Z. He, Y. Huang, A.-C. Shi, K. Jiang, Phase behavior of x-shaped liquid crystalline macromolecules. *J. Chem. Phys.* **162**, 114904 (2025).
118. A. Petrov, G. A. Hernández-Mendoza, A. Alexander-Katz, Symmetric diblock copolymers form versatile and switchable ultrasmall nanoparticles. *ACS Nano* **19**, 3665–3675 (2025).
119. C. Cai, L. Zhang, J. Lin, L. Wang, Self-assembly behavior of pH- and thermosensitive amphiphilic triblock copolymers in solution: Experimental studies and self-consistent field theory simulations. *J. Phys. Chem. B* **112**, 12666–12673 (2008).
120. K. Katsov, M. Müller, M. Schick, Field theoretic study of bilayer membrane fusion. I. Hemifusion mechanism. *Biophys. J.* **87**, 3277–3290 (2004).
121. S. Kim, P. F. Nealey, F. S. Bates, Decoupling bulk thermodynamics and wetting characteristics of block copolymer thin films. *ACS Macro Lett.* **1**, 11–14 (2012).
122. X. Wei, W. Chen, X. Chen, T. P. Russell, Disorder-to-order transition of diblock copolymers induced by alkyne/azide click chemistry. *Macromolecules* **43**, 6234–6236 (2010).
123. H. Feng *et al.*, Synthesis and characterization of amine-epoxy-functionalized polystyrene- block -poly(glycidyl methacrylate) to manage morphology and covarying properties for self-assembly. *Macromolecules* **56**, 2675–2685 (2023).
124. H. Feng *et al.*, Optimized design of block copolymers with covarying properties for nanolithography. *Nat. Mater.* **21**, 1426–1433 (2022).
125. P. Mansky, Y. Liu, E. Huang, T. P. Russell, C. Hawker, Controlling polymer-surface interactions with random copolymer brushes. *Science* **275**, 1458–1460 (1997).
126. A. K. Mishra *et al.*, Gallol-based block copolymer with a high Flory-Huggins interaction parameter for next-generation lithography. *Macromolecules* **55**, 10797–10803 (2022).
127. S. Antoine *et al.*, Non-intuitive trends in Flory-Huggins interaction parameters in polyether-based polymers. *Macromolecules* **54**, 6670–6677 (2021).
128. S. Maekawa *et al.*, Chemically tailored block copolymers for highly reliable sub-10-nm patterns by directed self-assembly. *Nat. Commun.* **15**, 5671 (2024).
129. O. Xie, A. E. Cohen, B. D. Olsen, scft-id. GitHub. https://github.com/olsenlabmit/scft-id. Deposited 21 October 2025.
130. O. Xie, A. E. Cohen, Structure files for "Learning nature's assembly language with polymers." Zenodo. https://zenodo.org/records/15756493. Deposited 27 June 2025.
131. O. Xie, A. E. Cohen, Converged results of "Learning nature's assembly language with polymers." Zenodo, https://zenodo.org/records/15756753. Deposited 27 June 2025.